ACS Energy LETTERS

Cite This: ACS Energy Lett. 2017, 2, 2625-2634

http://pubs.acs.org/journal/aelccp

PERSPECTIVE

Ionic Processes in Water Electrolysis: The Role of Ion-Selective Membranes

S. Z. Oener,*,† S. Ardo,‡,§ and S. W. Boettcher*,†

†Department of Chemistry and Biochemistry, University of Oregon, Eugene, Oregon 97403, United States

‡Department of Chemistry and §Department of Chemical Engineering and Materials Science, University of California Irvine, Irvine, California 92697, United States

ABSTRACT: **Ionic separation and recombination processes in water electrolysis and fuel cell devices are of equal importance as the electron transfer processes that occur at the electrode surfaces. We illustrate the basic thermodynamic concepts governing the flow of ions in electrolyzer and fuel cell systems and the effects of pH gradients on the electrochemical phenomena. Particularly, we focus on the use of bipolar membranes, which are composed of anion- and cation-selective membranes enabling operation with different pH environments at the anode versus the cathode. The use of bipolar membranes thus broadens the materials' availability and could enable low-cost electrolysis systems that operate at very high efficiency. We end by discussing different materials and highlighting key gaps needed to realize such a system.**

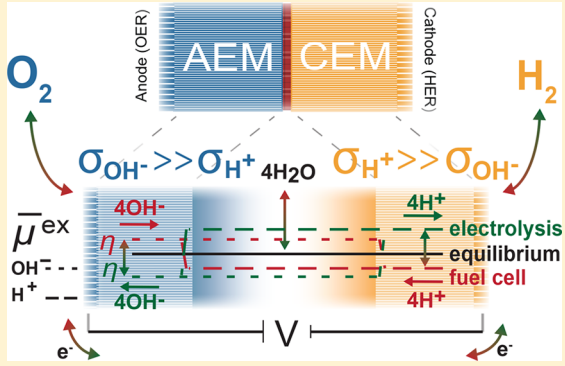

Catalytic fuel production from renewable energy sources and feedstocks is a promising approach for sustainable energy storage. The chemical fuels that are provided via catalysis can be safely stored for long times and exhibit the high-energy-density-to-weight ratio that is necessary for long-distance transportation.[1] Among those promising fuels, hydrogen has attracted interest from research and industrial communities due to its compatibility with a clean production-reaction cycle: water splitting stores electricity in hydrogen while fuel cell operation releases electricity via the reaction of hydrogen and oxygen forming water.[2,3] However, the application of this energy storage solution has been limited.

Fundamentally, among the key bottlenecks in improving water-splitting and fuel-cell technologies are the reaction kinetics, particularly the oxygen reduction and water oxidation reactions. A catalyst must provide ideal conditions for four separate electron-transfer steps involving four adsorbing intermediates on the catalyst's surface, all proceeding in series. Recently, several researchers have pointed out that it is important to engineer catalysts providing ideal local environments and adsorption energies for each of the four intermediates independently.[4−6] Systems must be developed that break the limitation that the binding energies of similar intermediates scale with the same materials' parameters.[7−9]

Many different material systems are available for potential oxygen evolution reaction (OER) and hydrogen evolution reaction (HER) catalysts, all possessing varying pH requirements for active and stable operation.[10−17] If the HER−OER catalyst pair operates at the same pH, spatial overlap of water dissociation with at least one of the two half-reactions is required. This means that at least one catalyst must drive water dissociation before the respective ion can be converted into O_2 or H_2 (see more discussion below).[18] Furthermore, on a microscopic scale, there are also challenges. For the HER on Pt, Ir, or Pd, the H-binding energy to the metal changes upon varying the pH from 0 to 14, resulting in a 100-fold decrease of the exchange current density.[19] For the OER, only a few expensive Ir- and/or Ru-based catalysts are known that show high and stable activity in acidic conditions at all, while the vast majority of OER catalysts, including ones from inexpensive materials such as $Ni(Fe)O_xH_y$, require basic conditions.[10,11,20−22] Recently, a few pH-universal catalysts have been developed that show promise in reducing pH constraints.[12,23−25] Importantly, the specific pH requirements for the HER−OER catalyst pair have substantial implications on the device level.

An integrated water-splitting device that operates the OER in base and the HER in acid is of particular interest. This would reduce the combined catalytic overpotentials and afford a large set of suitable catalysts. Figure 1a shows an integrated electrolysis device consisting of an additional water dissociation catalyst (red) sandwiched between an anion-exchange membrane (AEM, blue) and cation-exchange membrane (CEM, orange) that is fed by pure water. This bipolar membrane (BPM) configuration allows for direct application of the OER and HER catalysts on the outer AEM and CEM surfaces, respectively, and hence the formation of two triple-phase boundaries. Given sufficient ionic

Received: August 18, 2017
Accepted: October 10, 2017
Published: October 10, 2017

DOI: 10.1021/acsenergylett.7b00764
ACS Energy Lett. 2017, 2, 2625−2634

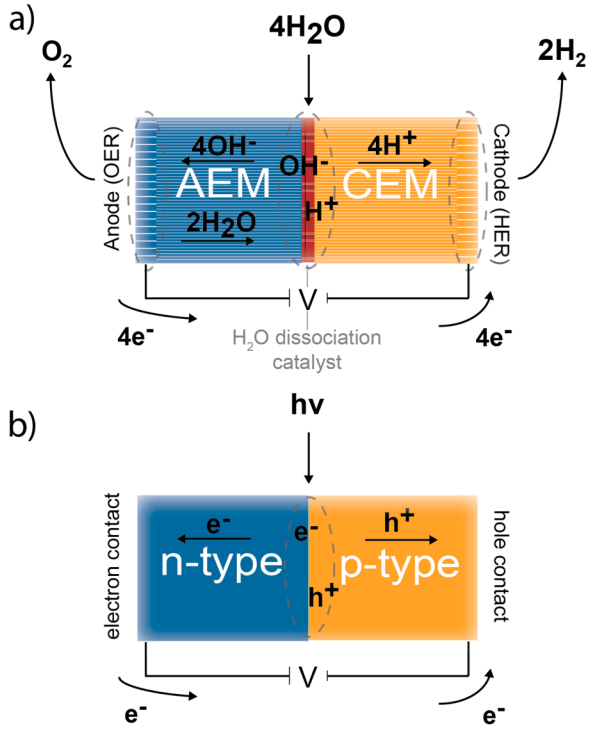

Figure 1. Integrated electrolysis device and traditional solar cell. (a) A water dissociation catalyst (red) is sandwiched between an AEM (blue) and CEM (orange). The OER and HER catalysts are directly applied on the two outer surfaces of this BPM, forming two triple-phase boundaries. The layer thicknesses are not drawn to scale. (b) Traditional solar cell with n- and p-type-doped regions that are selective to electrons and holes, instead of OH^- and H^+, respectively.

conductivities inside of the membranes, such a device can operate with pure feedwater, mitigating detrimental polarization gradients and membrane contamination from auxiliary ionic species, such as from salts and buffers. Furthermore, ion-exchange membranes effectively slow H_2 and O_2 product crossover.[26] For these reasons, BPMs have been used in both electrochemical and photoelectrochemical studies and have recently attracted renewed attention.[27−40]

Figure 1b shows the structure of a traditional solar cell as comparison. Instead of selectively transporting OH^- and H^+ as in the case of the AEM and CEM, respectively, the n- and p-type-doped semiconductor regions selectively transport e^- and h^+.

In the following, we discuss the basic thermodynamic working principles of integrated water-splitting device fed by pure water and focus on those that sustain a pH gradient between the HER and OER half-reactions. For such systems, ion-selective membranes that provide high ionic conductivity and effectively ideal local pH values at the active sites of catalysts are crucial components. We discuss different materials and highlight key gaps needed to enable the utilization of a system as in Figure 1. While we focus on electrolysis, the basic working principles hold true for the catalytic production of other fuels,[40] as well as for fuel-cell operation,[41] assuming that pure water is a reactant or product of the electrochemical reactions.

Kohl and co-workers have investigated the same system in Figure 1 with the focus on fuel-cell operation.[42−44] Recently, in analogy to semiconductor junctions and based on the formation of a Poisson−Nernst−Planck theory, Grew et al. provided in-depth information about the physical processes at the critical AEM−CEM interface. For a fuel cell, high ionic recombination rates in the junction region are of prime importance to support high current densities for a BPM-based system. Grew et al.'s analysis shows that bimolecular recombination processes are not sufficient to explain the high recombination rates that have been observed in experimental studies. Only additional trap-assisted recombination, e.g., via columbic interaction between mobile ions and fixed ionic charges (at the membrane surfaces), enables the required high recombination rates. Ahlfield et al. have investigated the BPM junction experimentally.[42] A large influence on the membrane resistance was found from the exact location of the junction within the BPM. Formation of the junction by applying an anion exchange ionomer directly on the surface of a CEM resulted in an improved current output in comparison to demonstrations where the junction was located in the center of the membrane. While membrane conductivity is equally important for membrane-based fuel-cell and electrolysis devices, the role of the ionic recombination in fuel cells (i.e., H^+ and OH^- to form water) is replaced by water dissociation and ionic separation (via water dissociation) in electrolysis devices (assuming that OER is driven at the AEM side to take advantage of earth-abundant alkaline stable catalysts). This situation will therefore be discussed in more detail below.

Electrolysis Basics. Water splitting proceeds via the HER and OER half-reactions. Depending on the pH of the electrolyte, the two half-reactions are given by the following equations (referenced to the standard hydrogen electrode, SHE:[45]

HER:

$$\text{pH 0: } 4H^+ + 4e^- \rightarrow 2H_2 \qquad E^0 = 0\ \text{V} \qquad (1)$$

$$\text{pH 14: } 4H_2O + 4e^- \rightarrow 2H_2 + 4OH^- \qquad E^0 = -0.83\ \text{V} \qquad (2)$$

OER:

$$\text{pH 0: } 2H_2O \rightarrow O_2 + 4H^+ + 4e^- \qquad E^0 = 1.23\ \text{V} \qquad (3)$$

$$\text{pH 14: } 4OH^- \rightarrow O_2 + 2H_2O + 4e^- \qquad E^0 = 0.40\ \text{V} \qquad (4)$$

From these equations, it is apparent that besides the transport of water and gas products, an integrated water-splitting device that links the HER and OER efficiently also needs to deliver the required electronic charge carrier type and the correct ion type to the respective reaction center. The OER requires the removal of electrons and the presence of OH^-, and therefore, in acid (eq 3), the OER is preceded by water dissociation. Likewise, HER requires the presence of H^+ and electrons, and therefore, in base, the HER is preceded by water dissociation (eq 2). In any case, all H^+ and OH^- originate from H_2O, even if acid, base, or salt is present. The presence of coupled electronic and ionic charge carriers at each electrode is an intrinsic property for energy conversion processes such as water-splitting devices and batteries. Solar cells in contrast only require spatial asymmetry of electronic charge carriers via two carrier-selective contacts (in traditional solar cells, the n- and p-doped semiconductor regions).[46] For electrochemical water splitting, the electronic asymmetry can be easily achieved if electrically biased electrodes are spatially separated in solution.

Electric asymmetry is sufficient for water splitting if the OER−HER catalyst pair does not require a pH difference for stable and active operation ($\Delta pH = 0$). As a result, at least one of the two half-reactions necessarily overlaps spatially with water

DOI: 10.1021/acsenergylett.7b00764
ACS Energy Lett. 2017, 2, 2625−2634

dissociation (either before, after, or simultaneously with electron transfer). This can be seen, for example, for the HER−OER couple according to eqs 1 and 3. Even though the OER reaction consumes OH^-, most OH^- ions are bound to H^+ and are transported as the neutral water molecule; only at the OER catalyst is OH^- dissociated from H_2O and oxidized. If the two half-reactions are proceeding in less extreme pH regions, e.g., due to catalyst stability constraints, including additional salts is necessary to increase the low intrinsic conductivity of water. Furthermore, the system must maintain a specific range of H^+ and OH^- concentrations, e.g., by employing a pH buffer that prevents large pH gradients from forming, although concentration gradients in the buffer can form and reduce the efficiency.

For OER−HER catalyst pairs that require a pH difference ($\Delta pH \neq 0$), ion-selective contacts are essential components of a sustainable integrated device. Figure 2a shows the well-known Nernstian potential pH dependence of the OER (red line) and HER (blue line). The difference between the two half-reactions ($E_{e-} = E_{cathode\ e-} - E_{anode\ e-}$) is the electrochemical potential that has to be afforded to transfer electrons at the electrodes, and it varies depending on the respective pH of the two half-reactions and can even change sign at the (nonphysical) ΔpH of ~21. To sustain a pH gradient across the cell, a potential must be afforded to separate the ionic species (E_{sep}). In general, E_{sep} equals the membrane potential of two regions with varying pH and is equal to the Gibbs free energy of mixing divided by Faraday's constant. In contrast to regular junction potentials that develop during operation due to differences in conductivity of the involved species,[47] E_{sep} does not depend on the transference numbers of OH^- and H^+; it is thermodynamic in nature and depends only on the absolute OH^- and H^+ concentrations.[43,44]

> Water splitting can be considered as consisting of at least two distinct steps, the separation of water into H^+ and OH^- and the transfer/separation of electrons at the electrodes.

Figure 2b shows the relation between the two potential contributions E_{sep} (blue line) and E_{e-} (orange line) to the total potential $E^0_{tot} = -1.23$ V (green line) for water splitting. E^0_{tot}, E_{sep}, and E_{e-} denote potential differences at electrochemical equilibrium. Those differences are a direct measure of the free-energy change $\Delta G_{tot} = -nFE_{tot} = -nF(E_{sep} + E_{e-}) = \Delta G_e + \Delta G_{sep}$. Externally supplying a pH difference of >21 units and in the correct direction (with the smaller pH value on the HER side) results in spontaneous hydrogen and oxygen production from the strong acid and base, respectively (green shaded area); however, the total potential at 1 bar H_2 and O_2 and 25 °C is still given by $E^0_{tot} = -1.23$ V if one includes the energy of creating the external supply of acid and base. Figure 2a,b supports the notion that water splitting can be considered as consisting of at least two distinct steps, the separation of water into H^+ and OH^- and the transfer/separation of electrons at the electrodes. Only at $\Delta pH = \sim 21$ ($E_{e-} = 0$ V) is the reaction solely dictated by the energetics of proton and hydroxide separation, and only at $\Delta pH = 0$ ($E_{sep} = 0$ V) is the reaction solely dictated by the energetics of electron separation at the electrodes. Importantly, the ionic and electronic separations are both driven by differences in electrochemical potentials due to the intrinsic linkage of charge and the number for electric and ionic charge carriers.

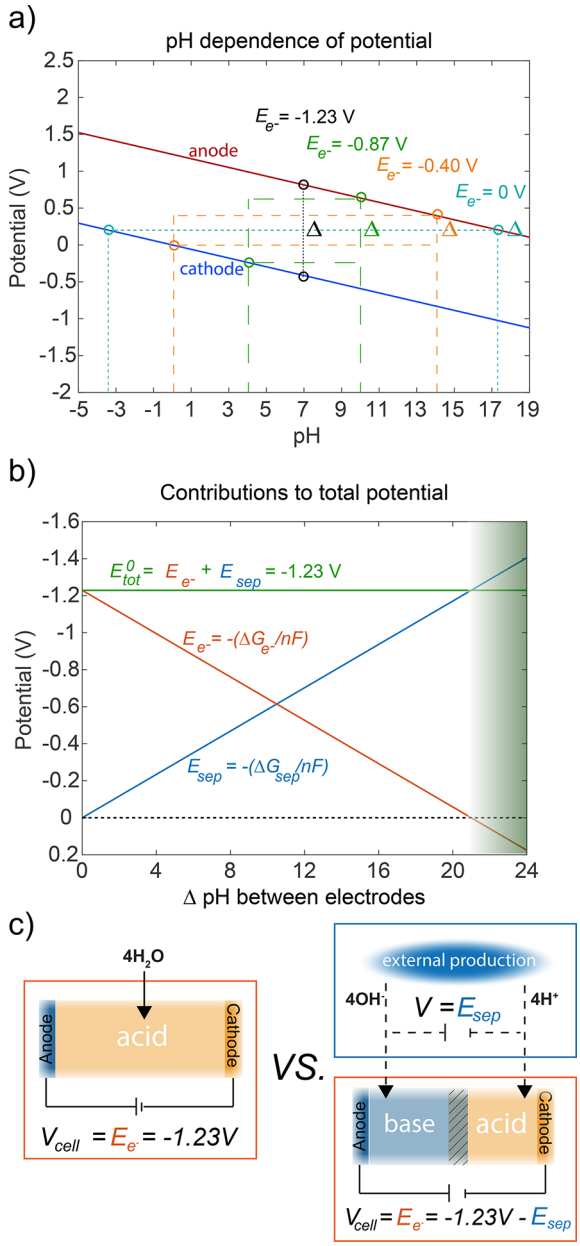

Figure 2. Influence of pH and ionic separation on the Nernstian potential. (a) pH dependence of the Nernstian potential at electrodes (E_{e-}) for the OER (red line) and HER (blue line). (b) Contribution of ionic separation E_{sep} (blue line) and E_{e-} (orange line) to the total potential $E^0_{tot} = -1.23$ V (green line) for water splitting as a function of $\Delta pH = pH_{anode} - pH_{cathode}$. For ΔpH > ~21, electrolysis would occur spontaneously at the electrodes (green shaded area) if the pH gradient and hence free energy $\Delta G_{sep} = nFE_{sep}$ are externally supplied. (c) Schematic emphasizing the difference in cell potential. On the left side, the total cell potential is $V_{cell} = E_{e-} = -1.23$ V. On the right side, $V_{cell} = E_{e-} = -1.23$ V $- E_{sep}$, while E_{sep} is supplied via the pH gradient of the preceding separation of OH^- and H^+ by affording ΔG_{sep}. The system on the right builds up salt ions, OH^-, and H^+ gradients, causing current opposite to the desired direction, part of which can be avoided by a porous separator (dashed lines).

Figure 2c depicts the cell potential (V_{cell}) under conditions where pure water is the feed (left) and acid/base are the feeds (right) and oxygen and hydrogen gases are present at the anode and cathode, respectively. On the left side of Figure 2c, the cell potential is $V_{cell} = -1.23$ V, with no net current, while on the right

DOI: 10.1021/acsenergylett.7b00764
ACS Energy Lett. 2017, 2, 2625−2634

side, the cell potential is $V_{cell} = E_{e-} = -1.23\ V - E_{sep}$. In the latter case, the ionic separation has taken place externally and is not accounted for by V_{cell}. The system on the left only requires neutral water input, while the system on the right requires continuous supply of H^+ and OH^-, which are generated/separated externally. This implies that systems that rely on continuous acid and base supply are in fact externalizing the energetic costs (ΔG_{sep}) of H^+ and OH^- separation to the commercial production of base and acid. Only considering the cell potential (V_{cell}) falls short of an accurate energetic assessment. Therefore, irrespective of where H^+ and OH^- separation occurs, the potential E_{sep} always has to be included, in which case, $E^0_{tot} = E_{e-} + E_{sep} = -1.23$ V always (at 1 bar H_2 and O_2 and 25 °C). The system on the left side of Figure 2c is strictly limited to ΔpH = 0 between the electrodes. By utilizing a BPM (more below), a pH gradient can be maintained sustainably in an integrated device.

> Systems that rely on continuous acid and base supply are in fact externalizing the energetic costs (ΔG_{sep}) of H^+ and OH^- separation to the commercial production of base and acid.

Figure 3 depicts current−potential curves for electrolysis (green lines, $V > V_{oc}$) with external acid and base supply (1, dotted lines) and with integrated water dissociation and ion separation across a BPM (2, solid line). For fuel-cell operation (red lines, $V < V_{oc}$), the dotted I−V curve represents the generation of acid and base and their removal to the exterior. In general, any unbalanced external production of H^+ and OH^-, e.g., sulfuric acid coupled to potassium hydroxide production, adds additional free-energy costs.

Membranes. Devices utilizing a BPM, such as in Figure 3 on the right, require only pure water as input and integrate water dissociation and ionic separation. While the water dissociation proceeds in the BPM junction region, the two oppositely polarized membranes, the CEM and AEM, are the essential components providing ionic separation via ion-selective transport.[43]

Figure 4 depicts the oppositely polarized nanochannels with cationic (blue) and anionic surface charge (orange). The

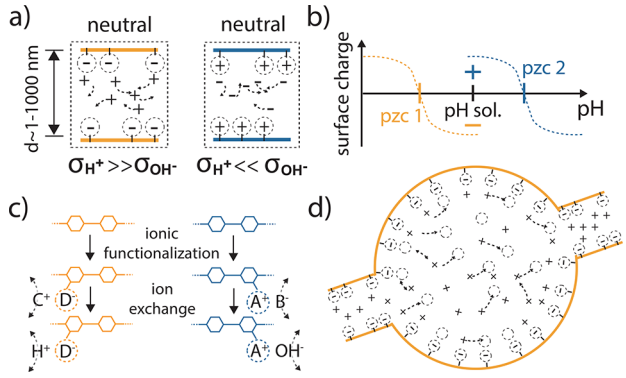

Figure 4. Conduction mechanism in ion-selective membranes. (a) Individual channels with cationic (blue) and anionic surface charge (orange). For channel diameters in the range of $d \approx 1-1000$ nm (depending on the ionic strength of the solution), the conductivity is strongly influenced by (b) the pzc of the surface material and the pH of the solution, resulting in either a protonated (pH < pzc) or deprotonated inorganic surface (pH > pzc). As a result of the fixed ions, the Coulombic forces and Donnan equilibria lead to a strong concentration increase of the freely moving counterions in the channel center. (c) For organic membranes, charged functional groups are attached to the polymer chain followed by ionic exchange reactions to include H^+ or OH^- into the channel. Organic membranes often exhibit structural heterogeneity where they partition into two phases: hydrophilic channel domains (cavities) and hydrophobic regions. (d) Inside those domains, Grotthuss and vehicular conduction can lead to very high proton conductivities.

ion-selective conduction inside the channels originates from an inhomogeneous spatial distribution of ions in the channel interior while overall charge neutrality is still satisfied. The ion conduction inside a channel can deviate from bulk conduction substantially.[48−50] For channel diameters in the range of ~1−1000 nm (Figure 4a), the conduction can be influenced by the point of zero charge (pzc) of the intrinsic surface material and the pH of the solution, leading to either protonated (pH < pzc) or deprotonated surfaces (pH > pzc). For large pore sizes and high ionic strength solutions, the main conduction can still proceed via the bulk ionic concentration in the channel center and is only slightly altered by surface conduction due to the counterions; the channel has thus limited ionic selectivity.[51,52] However, with decreasing channel sizes, the electrical double layer overlaps

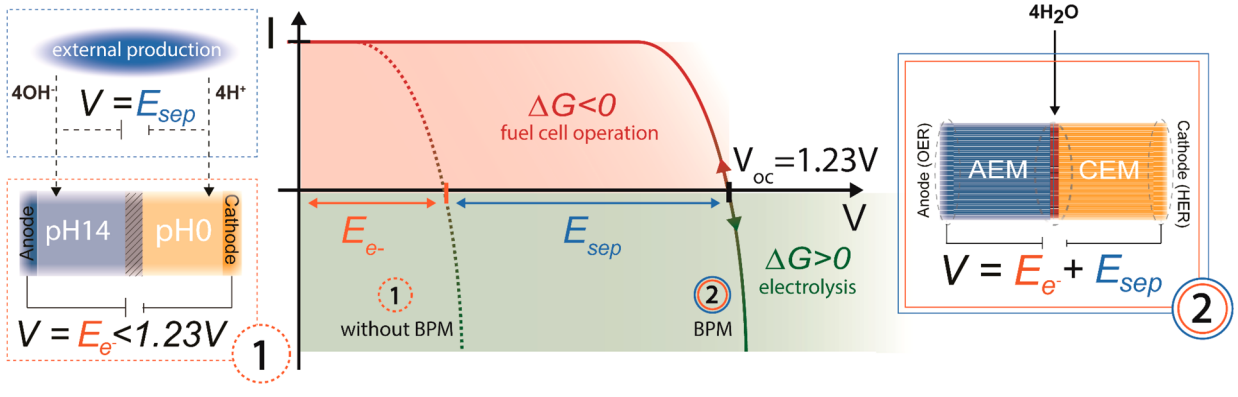

Figure 3. I−V curves for two different systems. Under reverse (green) and forward directions (red) for electrolysis and fuel-cell operation, respectively. In case of acid and base addition to (removal from) two separate compartments (1), the I−V curve is shifted due to the supplied (removed) free energy of ionic separation $\Delta G_{sep} = nFE_{sep}$ for electrolysis (fuel-cell operation). For systems that utilize a BPM (2), the ionic separation term E_{sep} is always integrated and only pure water supply is needed as input. The schematic assumes an ideal BPM, i.e., with ΔpH = 14 between the CEM and AEM, resulting in $E_{sep} \approx 830$ mV.

DOI: 10.1021/acsenergylett.7b00764
ACS Energy Lett. 2017, 2, 2625−2634

inside the nanochannel, which leads to a strong increase in counterion concentration in the channel center. As a result, the counterion conductivity increases and, thus, the channel's overall selectivity also increases (Figure 4b). This ion selectivity can also be described by Donnan exclusion effects.[53,54] Such conduction mechanisms have been investigated for intrinsic surface terminations in inorganic channels by the nanofluidics community.[55−59]

Organic materials are synthesized with controlled densities of charged functional groups (Figure 4c) and exhibit a complex internal structure. For example, according to the Gierke model, Nafion-like membranes are composed of nanochannel segments with diameters of ∼1 nm and larger hydrophilic cavities with diameters ∼4 nm (Figure 4d).[52] Depending on the degree of hydration,[60,61] those segments play a crucial role in the observed high proton conductivities. Two major conduction mechanisms have been identified; vehicular transport, i.e., solvation diffusion, and Grotthuss "hopping" through a hydrogen-bonded network, leading to largely increased mobilities.[50,52] Due to the nature of the hopping-like conduction, ionic ordering and water confinement effects have been investigated for their influence on the conduction mechanism.[30,62−66] In general, different transport models have been invoked that separate the membrane into phases of varying conductivities and that are able to describe conduction mechanisms that are influenced by material heterogeneity not only on the nanoscale but also on the microscale, e.g., in heterogeneous ion-exchange membranes.[52,67,68] Furthermore, we note that several improved models have been proposed to the Gierke model, e.g., by Kreuer,[69] which show more realistic geometric heterogeneity.[70]

Currently, CEMs, e.g., Nafion, are used in polymer−electrolyte membrane (PEM) fuel cells and electrolyzers.[26,50,71−74] The acidic conditions that result from use of Nafion necessitate that these PEM-based devices use expensive but stable noble-metal-containing catalysts (Pt, IrO_2). The required amount of noble metals continues to decrease due to optimization of the triple-phase boundary (TPB),[75,76] and new insights into the degradation mechanisms might increase the catalyst lifetime and lower the cost further.[77−82] Another option is to use stable and highly conductive AEMs that present basic conditions, thereby allowing use of base-stable non-noble metal catalysts for the ORR/OER. Realizing AEMs with these properties would lead to major breakthroughs for fuel cells and electrolyzers, among many other fields, such as redox flow batteries.[83] Several advances in AEMs have recently been reported, although more rapid development will require better control over degradation.[83−85] Several degradation mechanisms are known due to highly reactive OH^- ion attacking the bound cationic sites of the organic network. However, novel structures that utilize, e.g., steric shielding and high local electron densities are being investigated as promising candidates to overcome limitations.[83] Another approach may be to use chemically and thermally robust inorganic materials with relatively large nanochannels that were recently shown to exhibit Grotthuss conduction.[86,87] Future designs could include hybrid approaches using organic−inorganic materials that afford a vast parameter space of organic synthesis, allowing tunability in functionality and chemical robustness in combination with the high thermal stability of inorganic frameworks.

AEM limitations and proposed alternative options aside, fully integrated devices have been developed that utilize BPMs. Those devices allow operation of a catalyst pair under the presence of an internal pH gradient ($\Delta pH \neq 0$), which largely extends the set of available catalysts.[35,36,88−90] Furthermore, compared to systems relying on continuous external acid and base supply to sustain the pH gradient, ion-separating BPMs working in pure water provide simultaneous water dissociation and ion-selective contacts. However, with few exceptions,[43,44] BPMs have largely been used with bulk solutions of base and acid that contain counterions, which results in ionic crossover and loss of the pH gradient over time. Furthermore, additional salts and buffer are often required to raise the solution conductivity and sustain the pH at the metal electrodes, respectively, which can lead to additional polarization gradients of buffer species and thus to free-energy losses. In addition, concentrated salt solutions can negatively affect the stability of catalysts and they inevitably lead to diffusion of counterions into the membranes (where they are then termed co-ions) and thereby contamination and co-ion conduction.[31] Ideally, the catalysts for the two half-reactions would be directly applied onto the two outer surfaces of the BPM to establish two TPBs, mitigating many of the issues that arise when ions other than H^+ and OH^- are used.

Membranes effectively control charge on the nano- and subnanoscale, leading to pathways of strongly increased counterion conductivities: ion-selective contacts are established.

Membranes thus effectively control charge on the nano- and subnanoscale, leading to pathways of strongly increased counterion conductivities: ion-selective contacts are established. This situation is reminiscent of impurity doping in semiconductors to attain selective contacts for electrons and holes: charged impurity atoms are bound by the crystal lattice while the electric counter charge is free to move at room temperature on a pathway in space and energy, the conduction and valence bands.

Ion Selectivity and Thermodynamics. To understand the ion-selective properties of ion-conducting membranes in more detail, it is instructive to recall that the H^+ and OH^- current density J for constant pressure p is given by[47,52]

$$J_i^\alpha = -\frac{\sigma_i^\alpha}{q_i^\alpha}\cdot \mathrm{grad}(\bar{\mu}_i^\alpha) \tag{5}$$

$$\sigma_i^\alpha = q_i^\alpha \cdot n_i^\alpha \cdot m_i^\alpha \quad \text{and} \quad \bar{\mu}_i^\alpha = \mu_i^\alpha + q_i^\alpha \phi_i^\alpha \tag{6}$$

where σ is the ionic conductivity (ohm^{-1} cm^{-1}) with the charge per ion $q = z \cdot e$ (C/particle), the concentration n (particles/cm^3) and the mobility m (cm^2 V^{-1} s^{-1}). z is the unitless charge number and sign, $\bar{\mu}$ is the electrochemical potential, μ the chemical potential (both in J/particle) and ϕ is the electric potential (V). The subscript i denotes the particle type (OH^-, H^+, e^- or h^+), the superscript α denotes the phase (anode, solution near anode, etc.). Due to the serial nature of the processes, electric currents in the electrodes must be matched by ionic currents in each phase, e.g., $J^{\mathrm{anode}} = J^{\mathrm{cathode}} = J'_{\mathrm{OH-}} + J'_{\mathrm{H+}}$. Equations 5 and 6 imply that ion separation for species i occurs at an interface between two phases α and β if $\sigma_i^\alpha \cdot \mathrm{grad}(\bar{\mu}_i^\alpha) \neq \sigma_i^\beta \cdot \mathrm{grad}(\bar{\mu}_i^\beta)$, that is, if the current in phase α cannot be matched by the current in phase β. An ion-selective contact, e.g., phase α, supports the current for species i while suppressing it for species j, that is, $\sigma_i^\alpha \cdot \mathrm{grad}(\bar{\mu}_i^\alpha) \gg \sigma_j^\alpha \cdot \mathrm{grad}(\bar{\mu}_j^\alpha)$. Ion selectivity can be achieved if the conductivities for OH^- ions differ largely from the ones for H^+ ions. This is the case for fast ion-conducting membranes, such as AEMs and CEMs,

DOI: 10.1021/acsenergylett.7b00764
ACS Energy Lett. 2017, 2, 2625−2634

which exhibit largely varying conductivities for OH^- and H^+, enabled by strongly differing concentrations and mobilities. The degree of selectivity is traditionally expressed by the permselectivity, as defined by Winger et al.[91]

Figure 5a shows an integrated electrolysis device whose integral parts are the two ion-selective membranes that provide an ideal local pH for the catalysts in direct contact with the respective electrode. Such a system has been investigated theoretically[43] and experimentally[42,44,92−94] for fuel-cell operation. Without loss of generality, we consider the case for which the HER (OER) at the cathode (anode) is proceeding in an acidic (basic) environment due to the tendency of HER (OER) catalysts to work better in that respective environment. As explained above, the pH at the cathode (anode) can be controlled by using a CEM (δ) (AEM (α)), which is dominated by H^+ (OH^-) counterion conduction in channels lined with fixed anionic (cationic) groups. As the water dissociation catalyst at $\beta|\gamma$ is positioned in close vicinity to the water−membrane interfaces ($\alpha|\beta$ and $\gamma|\delta$), the dissociated ions are separated due to the ion selectivity of the membranes. The ion-selective membranes are directly in contact with the respective HER/OER catalyst on the outer surface to avoid resistive and polarization losses in spatially extended bulk solutions of traditional systems. Consequently, a TPB (TPB^a and TPB^c) is established at the surface of each membrane between the evolved gas species, the dissolved H^+/OH^-, and the electric charge carriers from the anode and cathode.[95] The TPBs require careful optimization in terms of catalyst density and porosity, ensuring ideal transport properties and catalyst activity, while the membrane ideally prevents transport of H_2 and O_2 gases (crossover) through the confined nanochannels and the membrane bulk material.[41,96,97] Importantly, the direct application of a cathode to a CEM and the established TPB is employed in CEM fuel cells and electrolyzers, as well as AEM fuel cells.[72−74] Noteworthy, in the initial development stages of PEM fuel cells, the membrane was separated by an acid contact layer from the catalyst before systems were substantially improved and simplified by removing the acid layer.[50]

At the open-circuit voltage, V_{oc}, the electrochemical potential of TPB^a (TPB^c) is aligned to the potential of the anode (cathode). The system has free energy stored in H_2 and O_2 at 1 bar that can be released by operating the system at a voltage $V < V_{oc}$, that is, as a fuel cell $\Delta G = -nF(V_{oc} - V) < 0$. At a voltage $V > V_{oc}$, additional free energy is added to the system and electrolysis takes place with $\Delta G > 0$. Instead of showing the absolute constant electrochemical potentials at V_{oc} for OH^- and H^+ on the same scale in Figure 5a, we adopt the definition of the excess electrochemical potentials ($\bar{\mu}^{ex}$) in Figure 5b from Grew et al., who have provided detailed calculations for a fuel cell based on the same system as that in Figure 5.[43] According to this definition the excess quasi-electrochemical potentials

$$\bar{\mu}_i^{ex} = \bar{\mu}_i(C_i, \phi) - \bar{\mu}_i^0(C_i^0) \tag{7}$$

where $\bar{\mu}_i^0(C_i^0)$ denotes the electrochemical potential of species i (H^+ or OH^-) in neutral water at electrochemical equilibrium in the absence of any electrical field ϕ. Conversely, $\bar{\mu}_i(C_i, \phi)$ denotes the electrochemical potential at a specific state relative to the reference state. In analogy to the quasi-Fermi levels in solar cells, the excess electrochemical potentials allow one to describe the nonequilibrium condition for H^+ or OH^- on the same scale and visualize free-energy changes to the system relative to the reference state. However, in contrast to solar cells, the chemical potential difference giving rise to the open-circuit voltage is

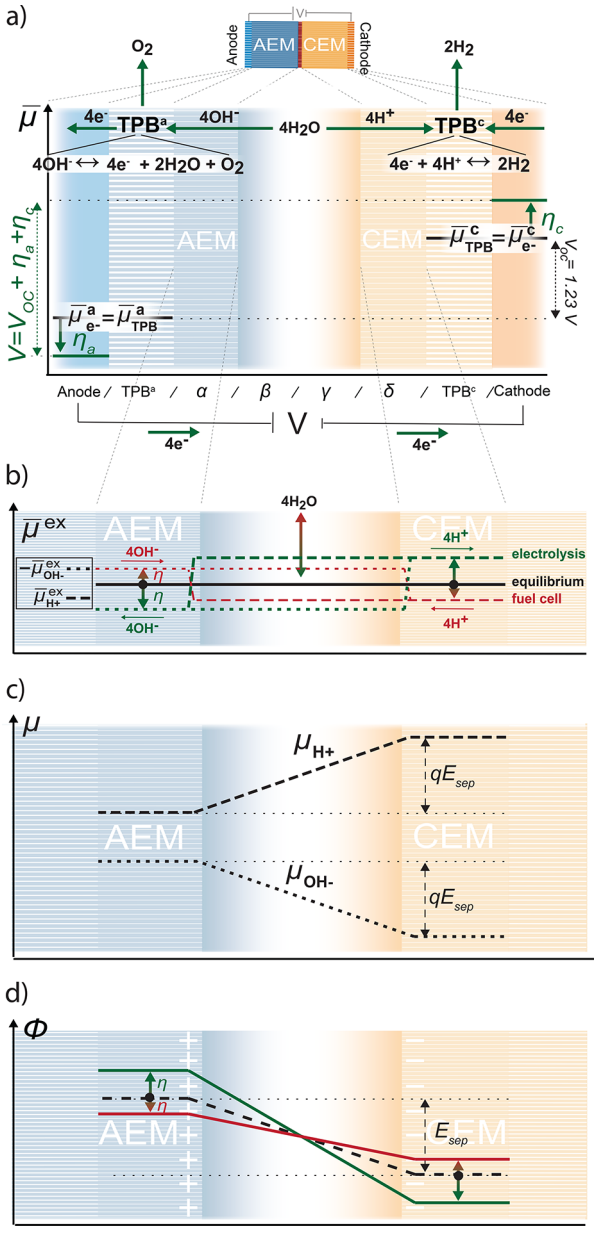

Figure 5. Electrolysis device incorporating a BPM. (a) Water is dissociated via a catalyst (at $\beta|\gamma$) followed by the separation of OH^- (β) and H^+ (γ) toward the respective ion-selective membranes (α, δ), which provide local pH values in direct contact with the respective electrode. The water dissociation catalyst must be positioned in close vicinity to the water−membrane interfaces, avoiding recombination and facilitating ion separation by gradients in electrochemical potentials and ion-selective membrane conduction. (b) Schematic of the excess electrochemical potentials (defined in the text) for the different regions of the electrolyte in panel (a) for water electrolysis (green, $\Delta G > 0$) and fuel-cell (red, $\Delta G < 0$) operation. For clarity, the schematic shows the extreme case for which the junction potential inside of the membrane is fully translated into splitting of the excess electrochemical potentials for OH^- and H^+ due to large overpotentials. When in electrochemical equilibrium, (c) the chemical potential of OH^- and H^+ is compensated by (d) the electric potential (dashed black lines). During water electrolysis (green), the electric potential difference increases, while it decreases during fuel-cell operation (red). The ionic separation term E_{sep} is established between the two membranes (α and δ), i.e., it is spatially separated from the respective electrode surfaces.

DOI: 10.1021/acsenergylett.7b00764
ACS Energy Lett. 2017, 2, 2625−2634

located outside of the ion-separating BPM, instead of inside as in the analogous case of the light-absorbing and charge-separating semiconductor. As a result, for fuel cells and electrolysis devices at V_{oc}, the excess electrochemical potentials for H^+ and OH^- are constant and equal to each other and the thermal equilibrium concentrations of OH^- /H^+ are established according to $[OH^-][H^+] = K_W(T) = k_d/k_a$. However, with applied membrane overpotential positive or negative to the V_{oc} the limited water dissociation (small exchange current for the water dissociation/association processes) and additional practical transport limitations give rise to the occurrence of splitting of the excess electrochemical potentials for H^+ and OH^-. Figure 5b shows the extreme case for which the junction potential inside of the membrane is fully translated into splitting of the excess electrochemical potentials for OH^- and H^+.

Similar to solar cells, the occurrence of excess electrochemical potentials for H^+ and OH^- has important implications for ion separation via ion-selective membranes. Ideally, applying an electrochemical potential gradient directly translates into ion separation according to eq 5; due to the gradient, H^+ and OH^- would move in opposite directions even for equal conductivities in all phases. However, as described above, with increasing overpotentials across the membrane, the excess electrochemical potentials for H^+ and OH^- split increasingly from each other. As a result of this increased splitting (e.g., red or green dashed lines in Figure 4b), the excess electrochemical potential gradients for H^+ and OH^- at the water−membrane interfaces decrease compared to the theoretical case of vanishing splitting at an applied overpotential. Thus, with increasing overpotentials, the charge separation increasingly relies on the different conductivities for H^+ and OH^- inside of each membrane to establish the required current asymmetry, i.e, $\sigma^{\alpha}_{OH^-} \cdot \nabla\bar{\mu}^{\alpha}_{OH^-} \gg \sigma^{\alpha}_{H^+} \cdot \nabla\bar{\mu}^{\alpha}_{H^+}$ and $\sigma^{\omega}_{OH^-} \cdot \nabla\bar{\mu}^{\omega}_{OH^-} \ll \sigma^{\omega}_{H^+} \cdot \nabla\bar{\mu}^{\omega}_{H^+}$. This situation is similar to a solar cell for which charge carrier-selective contacts are of prime importance for efficient operation.[46,98,99]

Figure 5c and d show the chemical potential and electric potential, respectively. At electrochemical equilibrium (black dashed lines), the electric potential compensates the chemical potential fully. The ionic separation term of the total potential (E_{sep}) is established between the two membranes α and δ, i.e., it is spatially separated from the respective electrode reactions (E_{e-}), in contrast to regular electrode assemblies operating at a single pH. Applying an overpotential η negative (positive) of the V_{oc} during fuel-cell (electrolysis) operation leads to changing electric potentials in the respective direction. One might be tempted to state that the electric potential gradient, i.e., electric field, at equilibrium causes the separation of H^+ and OH^-. However, this wrong description neglects the chemical potential gradient, which compensates the electric potential gradient at equilibrium; unless one of the two potentials is strictly zero, an accurate description can only be obtained via the electrochemical potential gradient due to the intrinsic connection of charge and number for electronic as well as ionic charge carriers. Nonetheless, at nonequilibrium conditions with an applied overpotential driving water dissociation, the electric field inside of the few-nanometer-thin interfacial layer can become very large (Figure 5d). This condition has led to the development of theory invoking Onsager's theory of the second Wien effect to explain the experimentally observed high water dissociation rates in BPMs even in the absence of additional water dissociation catalysts.[100−103]

The here-discussed intrinsic reversibility utilizing the very same device for both modes is essentially the working principle of unitized regenerative fuel cells (so far only at ΔpH = 0).[104−107] By allowing operation of a single device either in water-splitting or in fuel-cell mode, the total system costs of an integrated energy storage solution could be largely reduced. However, currently, the large costs associated with the catalysts and the membrane stack and especially the balance of plant (water, gas and heat management) are large obstacles for terrestrial commercialization, while space applications are being investigated.[108,109]

Summary and Future Outlook. We discussed integrated electrolysis and fuel-cell devices that operate the OER/ORR and HER/HOR at different pH values to reduce the combined overpotentials and increase the set of available catalysts. For such systems, ion-selective contacts that efficiently sustain a pH gradient across the device and provide ideal local environments for the catalysts are important. Membrane-based systems that utilize two triple-phase boundaries for an integrated device instead of bulk solutions and operate in pure water potentially avoid not only product crossover but also polarization gradients, membrane contamination, and co-ion conduction. On the basis of those fundamental advantages, we stress the importance of the development of novel membranes for future electrolysis and fuel-cell commercialization, in particular, the development of stable and highly conducting AEMs. The commercial success of the PEM fuel cell enabling stable operation, reduced overpotentials and polarization gradients, compactness, and intrinsically safe operation underlines the importance of future research on membranes for low- and high-temperature electrolysis and fuel cells.

Membrane-based systems that utilize two triple-phase boundaries for an integrated device instead of bulk solutions and operate in pure water potentially avoid not only product crossover but also polarization gradients, membrane contamination, and co-ion conduction.

AUTHOR INFORMATION

Corresponding Authors

*E-mail: szo@uoregon.edu (S.Z.O.).
*E-mail: swb@uoregon.edu (S.W.B.).

ORCID

S. Ardo: 0000-0001-7162-6826
S. W. Boettcher: 0000-0001-8971-9123

Author Contributions

All authors contributed to the manuscript.

Notes

The authors declare no competing financial interest.

Biographies

Dr. Sebastian Z. Oener is a postdoctoral researcher at the University of Oregon, working on electrocatalysis for long-term energy storage. He studied physics at the University of Constance, Germany, and at Massachusetts Institute of Technology, U.S.A. He obtained his Ph.D. from AMOLF in Amsterdam, The Netherlands, working on nano-photovoltaics.

Dr. Shane Ardo is an Assistant Professor of Chemistry, and Chemical Engineering and Materials Science, at the University of California,

DOI: 10.1021/acsenergylett.7b00764
ACS Energy Lett. 2017, 2, 2625−2634

Irvine. He received his B.S. degree in mathematics from Towson University in 1999, M.S. degree in nutrition from the University of Maryland, College Park in 2005, and M.A. and Ph.D. degrees in chemistry from the Johns Hopkins University in 2008 and 2010, respectively, before performing postdoctoral work at the California Institute of Technology.

Dr. Shannon W. Boettcher is a Associate Professor of Chemistry at the University of Oregon. He received his B.A. at the University of Oregon in 2003 and his Ph.D. at UC Santa Barbara in 2008. His postdoctoral work was at the California Institute of Technology. His group focuses on the fundamental aspects of solar energy conversion and storage. More information can be found at http://boettcher.uoregon.edu.

■ ACKNOWLEDGMENTS

This work was supported by the National Science Foundation Chemical Catalysis program under Grant CHE-1566348, by the Research Corporation for Science Advancement, the Alfred P. Sloan Foundation, and the Dreyfus Foundation.

■ REFERENCES

(1) Lewis, N. S. Research Opportunities to Advance Solar Energy Utilization. *Science* **2016**, *351*, aad1920−aad1920.
(2) Brandon, N. P.; Kurban, Z. Clean Energy and the Hydrogen Economy. *Philos. Trans. R. Soc., A* **2017**, *375*, 20160400.
(3) Lewis, N. S. Powering the Planet. *MRS Bull.* **2007**, *32*, 808−820.
(4) Vojvodic, A.; Nørskov, J. K. New Design Paradigm for Heterogeneous Catalysts. *Natl. Sci. Rev.* **2015**, *2*, 140−143.
(5) Doyle, A. D.; Montoya, J. H.; Vojvodic, A. Improving Oxygen Electrochemistry through Nanoscopic Confinement. *ChemCatChem* **2015**, *7*, 738−742.
(6) Medlin, J. W.; Montemore, M. M. Scaling the Rough Heights. *Nat. Chem.* **2015**, *7*, 378−380.
(7) Busch, M.; Wodrich, M. D.; Corminboeuf, C. Linear Scaling Relationships and Volcano Plots in Homogeneous Catalysis − Revisiting the Suzuki Reaction. *Chem. Sci.* **2015**, *6*, 6754−6761.
(8) Abild-Pedersen, F.; Greeley, J.; Studt, F.; Rossmeisl, J.; Munter, T. R.; Moses, P. G.; Skúlason, E.; Bligaard, T.; Nørskov, J. K. Scaling Properties of Adsorption Energies for Hydrogen-Containing Molecules on Transition-Metal Surfaces. *Phys. Rev. Lett.* **2007**, *99*, 4−7.
(9) Calle-Vallejo, F.; Loffreda, D.; Koper, M. T. M.; Sautet, P. Introducing Structural Sensitivity into Adsorption−energy Scaling Relations by Means of Coordination Numbers. *Nat. Chem.* **2015**, *7*, 403−410.
(10) Reier, T.; Nong, H. N.; Teschner, D.; Schlögl, R.; Strasser, P. Electrocatalytic Oxygen Evolution Reaction in Acidic Environments - Reaction Mechanisms and Catalysts. *Adv. Energy Mater.* **2017**, *7*, 1601275.
(11) McCrory, C. C. L.; Jung, S.; Ferrer, I. M.; Chatman, S. M.; Peters, J. C.; Jaramillo, T. F. Benchmarking Hydrogen Evolving Reaction and Oxygen Evolving Reaction Electrocatalysts for Solar Water Splitting Devices. *J. Am. Chem. Soc.* **2015**, *137*, 4347−4357.
(12) Stamenkovic, V. R.; Strmcnik, D.; Lopes, P. P.; Markovic, N. M. Energy and Fuels from Electrochemical Interfaces. *Nat. Mater.* **2016**, *16*, 57−69.
(13) Roger, I.; Shipman, M. A.; Symes, M. D. Earth-Abundant Catalysts for Electrochemical and Photoelectrochemical Water Splitting. *Nat. Rev. Chem.* **2017**, *1*, 0003.
(14) Yan, Y.; Xia, B. Y.; Zhao, B.; Wang, X. A Review on Noble-Metal-Free Bifunctional Heterogeneous Catalysts for Overall Electrochemical Water Splitting. *J. Mater. Chem. A* **2016**, *4*, 17587−17603.
(15) Anantharaj, S.; Ede, S. R.; Sakthikumar, K.; Karthick, K.; Mishra, S.; Kundu, S. Recent Trends and Perspectives in Electrochemical Water Splitting with an Emphasis on Sulfide, Selenide, and Phosphide Catalysts of Fe, Co, and Ni: A Review. *ACS Catal.* **2016**, *6*, 8069−8097.
(16) Mistry, H.; Varela, A. S.; Kühl, S.; Strasser, P.; Cuenya, B. R. Nanostructured Electrocatalysts with Tunable Activity and Selectivity. *Nat. Rev. Mater.* **2016**, *1*, 16009.
(17) Seh, Z. W.; Kibsgaard, J.; Dickens, C. F.; Chorkendorff, I.; Nørskov, J. K.; Jaramillo, T. F. Combining Theory and Experiment in Electrocatalysis: Insights into Materials Design. *Science* **2017**, *355*, eaad4998.
(18) Jiao, Y.; Zheng, Y.; Jaroniec, M.; Qiao, S. Z. Design of Electrocatalysts for Oxygen- and Hydrogen-Involving Energy Conversion Reactions. *Chem. Soc. Rev.* **2015**, *44*, 2060−2086.
(19) Durst, J.; Siebel, A.; Simon, C.; Hasché, F.; Herranz, J.; Gasteiger, H. A. New Insights into the Electrochemical Hydrogen Oxidation and Evolution Reaction Mechanism. *Energy Environ. Sci.* **2014**, *7*, 2255−2260.
(20) Trotochaud, L.; Young, S. L.; Ranney, J. K.; Boettcher, S. W. Nickel−Iron Oxyhydroxide Oxygen-Evolution Electrocatalysts: The Role of Intentional and Incidental Iron Incorporation. *J. Am. Chem. Soc.* **2014**, *136*, 6744−6753.
(21) Enman, L. J.; Burke, M. S.; Batchellor, A. S.; Boettcher, S. W. Effects of Intentionally Incorporated Metal Cations on the Oxygen Evolution Electrocatalytic Activity of Nickel (Oxy)hydroxide in Alkaline Media. *ACS Catal.* **2016**, *6*, 2416−2423.
(22) Burke, M. S.; Enman, L. J.; Batchellor, A. S.; Zou, S.; Boettcher, S. W. Oxygen Evolution Reaction Electrocatalysis on Transition Metal Oxides and (Oxy)hydroxides: Activity Trends and Design Principles. *Chem. Mater.* **2015**, *27*, 7549.
(23) Genorio, B.; Strmcnik, D.; Subbaraman, R.; Tripkovic, D.; Karapetrov, G.; Stamenkovic, V. R.; Pejovnik, S.; Marković, N. M. Selective Catalysts for the Hydrogen Oxidation and Oxygen Reduction Reactions by Patterning of Platinum with calix[4]arene Molecules. *Nat. Mater.* **2010**, *9*, 998−1003.
(24) Staszak-Jirkovský, J.; Malliakas, C. D.; Lopes, P. P.; Danilovic, N.; Kota, S. S.; Chang, K.; Genorio, B.; Strmcnik, D.; Stamenkovic, V. R.; Kanatzidis, M. G.; et al. Design of Active and Stable Co−Mo−Sx Chalcogels as pH-Universal Catalysts for the Hydrogen Evolution Reaction. *Nat. Mater.* **2015**, *15*, 197−203.
(25) Bae, J. H.; Kim, Y.-R.; Soyoung Kim, R.; Chung, T. D. Enhanced Electrochemical Reactions of 1,4-Benzoquinone at Nanoporous Electrodes. *Phys. Chem. Chem. Phys.* **2013**, *15*, 10645−10653.
(26) Kusoglu, A.; Weber, A. Z. New Insights into Perfluorinated Sulfonic-Acid Ionomers. *Chem. Rev.* **2017**, *117*, 987−1104.
(27) Berger, A.; Segalman, R. A.; Newman, J. Material Requirements for Membrane Separators in a Water-Splitting Photoelectrochemical Cell. *Energy Environ. Sci.* **2014**, *7*, 1468−1476.
(28) Verlage, E.; Hu, S.; Liu, R.; Jones, R. J. R.; Sun, K.; Xiang, C.; Lewis, N. S.; Atwater, H. A. A Monolithically Integrated, Intrinsically Safe, 10% Efficient, Solar-Driven Water-Splitting System Based on Active, Stable Earth-Abundant Electrocatalysts in Conjunction with Tandem III−V Light Absorbers Protected by Amorphous TiO_2 Films. *Energy Environ. Sci.* **2015**, *8*, 3166−3172.
(29) Ager, J. W.; Shaner, M. R.; Walczak, K. A.; Sharp, I. D.; Ardo, S. Experimental Demonstrations of Spontaneous, Solar-Driven Photoelectrochemical Water Splitting. *Energy Environ. Sci.* **2015**, *8*, 2811−2824.
(30) Chabi, S.; Papadantonakis, K. M.; Lewis, N. S.; Freund, M. S. Membranes for Artificial Photosynthesis. *Energy Environ. Sci.* **2017**, *10*, 1320−1338.
(31) Xiang, C.; Weber, A. Z.; Ardo, S.; Berger, A.; Chen, Y.; Coridan, R.; Fountaine, K. T.; Haussener, S.; Hu, S.; Liu, R.; et al. Modeling, Simulation, and Implementation of Solar-Driven Water-Splitting Devices. *Angew. Chem., Int. Ed.* **2016**, *55*, 12974−12988.
(32) Schreier, M.; Héroguel, F.; Steier, L.; Ahmad, S.; Luterbacher, J. S.; Mayer, M. T.; Luo, J.; Grätzel, M. Solar Conversion of CO2 to CO Using Earth-Abundant Electrocatalysts Prepared by Atomic Layer Modification of CuO. *Nat. Energy* **2017**, *2*, 17087.
(33) Zhou, X.; Liu, R.; Sun, K.; Chen, Y.; Verlage, E.; Francis, S. A.; Lewis, N. S.; Xiang, C. Solar-Driven Reduction of 1 Atm of CO_2 to Formate at 10% Energy-Conversion Efficiency by Use of a TiO_2

DOI: 10.1021/acsenergylett.7b00764
ACS Energy Lett. 2017, 2, 2625−2634

-Protected III−V Tandem Photoanode in Conjunction with a Bipolar Membrane and a Pd/C Cathode. *ACS Energy Lett.* **2016**, *1*, 764−770.
(34) Sun, K.; Liu, R.; Chen, Y.; Verlage, E.; Lewis, N. S.; Xiang, C. Solar-Driven Water Splitting: A Stabilized, Intrinsically Safe, 10% Efficient, Solar-Driven Water-Splitting Cell Incorporating Earth-Abundant Electrocatalysts with Steady-State pH Gradients and Product Separation Enabled by a Bipolar Membrane. *Adv. Energy Mater.* **2016**, *6*, 1−7.
(35) Luo, J.; Vermaas, D. A.; Bi, D.; Hagfeldt, A.; Smith, W. A.; Grätzel, M. Bipolar Membrane-Assisted Solar Water Splitting in Optimal pH. *Adv. Energy Mater.* **2016**, *6*, 1600100.
(36) Vermaas, D. A.; Sassenburg, M.; Smith, W. A. Photo-Assisted Water Splitting with Bipolar Membrane Induced pH Gradients for Practical Solar Fuel Devices. *J. Mater. Chem. A* **2015**, *3*, 19556−19562.
(37) Reiter, R. S.; White, W.; Ardo, S. Electrochemical Characterization of Commercial Bipolar Membranes under Electrolyte Conditions Relevant to Solar Fuels Technologies. *J. Electrochem. Soc.* **2016**, *163*, H3132−H3134.
(38) Gaieck, W.; Ardo, S. *Challenges and Opportunities for Ion-Exchange Membranes in Solar Fuels Devices* **2014**, *3*, 277−287.
(39) White, W.; Sanborn, C. D.; Fabian, D. M.; Ardo, S. Conversion of Visible Light into Ionic Power Using Photoacid-Dye-Sensitized Bipolar Ion-Exchange Membranes. *Joule* **2017**, Just Accepted.
(40) Li, Y. C.; Zhou, D.; Yan, Z.; Gonçalves, R. H.; Salvatore, D. A.; Berlinguette, C. P.; Mallouk, T. E. Electrolysis of CO_2 to Syngas in Bipolar Membrane-Based Electrochemical Cells. *ACS Energy Lett.* **2016**, *1*, 1149−1153.
(41) O'Hayre, R.; Cha, S.-W.; Colella, W.; Prinz, F. B. *Fuel Cell Fundamentals*; John Wiley & Sons, Inc: Hoboken, NJ, 2016.
(42) Ahlfield, J. M.; Liu, L.; Kohl, P. A. PEM/AEM Junction Design for Bipolar Membrane Fuel Cells. *J. Electrochem. Soc.* **2017**, *164*, F1165−F1171.
(43) Grew, K. N.; McClure, J. P.; Chu, D.; Kohl, P. A.; Ahlfield, J. M. Understanding Transport at the Acid-Alkaline Interface of Bipolar Membranes. *J. Electrochem. Soc.* **2016**, *163*, F1572−F1587.
(44) Ünlü, M.; Zhou, J.; Kohl, P. A. Hybrid Anion and Proton Exchange Membrane Fuel Cells. *J. Phys. Chem. C* **2009**, *113*, 11416−11423.
(45) Trasatti, S. The Absolute Electrode Potential: An Explanatory Note (Recommendations 1986). *Pure Appl. Chem.* **1986**, *58*, 955−966.
(46) Wuerfel, P.; Wuerfel, U. *Physics of Solar Cells: From Basic Principles to Advanced Concepts*, 3rd ed.; Wiley-VCH, 2016.
(47) Bard, A. J.; Faulkner, L. R. *Electrochemical Methods: Fundamentals and Applications*, 2nd ed.; Wiley, 2001.
(48) Tsukahara, T.; Mizutani, W.; Mawatari, K.; Kitamori, T. NMR Studies of Structure and Dynamics of Liquid Molecules Confined in Extended Nanospaces. *J. Phys. Chem. B* **2009**, *113*, 10808−10816.
(49) Chinen, H.; Mawatari, K.; Pihosh, Y.; Morikawa, K.; Kazoe, Y.; Tsukahara, T.; Kitamori, T. Enhancement of Proton Mobility in Extended-Nanospace Channels. *Angew. Chem., Int. Ed.* **2012**, *51*, 3573−3577.
(50) Kraytsberg, A.; Ein-Eli, Y. Review of Advanced Materials for Proton Exchange Membrane Fuel Cells. *Energy Fuels* **2014**, *28*, 7303−7330.
(51) Tanaka, Y.; Moon, S.-H.; Nikonenko, V. V.; Xu, T. Ion-Exchange Membranes. *Int. J. Chem. Eng.* **2012**, *2012*, 1−3.
(52) Nikonenko, V. V.; Yaroslavtsev, A. B.; Pourcelly, G. Ion Transfer in and Through Charged Membranes: Structure, Properties, and Theory. *Ionic Interactions in Natural and Synthetic Macromolecules*; John Wiley & Sons, Inc.: Hoboken, NJ, 2012; pp 267−335.
(53) Tanaka, Y. *Ion Exchange Membranes: Fundamentals and Applications*, 1st ed.; Elsevier, 2015.
(54) Donnan, F. G. Theory of Membrane Equilibria and Membrane Potentials in the Presence of Non-Dialysing Electrolytes. A Contribution to Physical-Chemical Physiology. *J. Membr. Sci.* **1995**, *100*, 45−55.
(55) Sparreboom, W.; van den Berg, A.; Eijkel, J. C. T. Principles and Applications of Nanofluidic Transport. *Nat. Nanotechnol.* **2009**, *4*, 713−720.
(56) Karnik, R.; Fan, R.; Yue, M.; Li, D.; Yang, P.; Majumdar, A. Electrostatic Control of Ions and Molecules in Nanofluidic Transistors. *Nano Lett.* **2005**, *5*, 943−948.
(57) Abgrall, P.; Bancaud, A.; Joseph, P. Nanofluidic Devices and Their Potential Applications. *Microfluid. Devices Nanotechnol. Fundam. Concepts* **2010**, *80*, 155−214.
(58) Van Der Heyden, F. H. J.; Stein, D.; Dekker, C. Streaming Currents in a Single Nanofluidic Channel. *Phys. Rev. Lett.* **2005**, *95*, 9−12.
(59) Lehovec, K. Space-Charge Layer and Distribution of Lattice Defects at the Surface of Ionic Crystals. *J. Chem. Phys.* **1953**, *21*, 1123−1128.
(60) Petersen, M. K.; Voth, G. A. Characterization of the Solvation and Transport of the Hydrated Proton in the Perfluorosulfonic Acid Membrane Nafion. *J. Phys. Chem. B* **2006**, *110*, 18594−18600.
(61) Anantaraman, A. V.; Gardner, C. L. Studies on Ion-Exchange Membranes. Part 1. Effect of Humidity on the Conductivity of Nafion®. *J. Electroanal. Chem.* **1996**, *414*, 115−120.
(62) Liu, L.; Bakker, H. J. Infrared-Activated Proton Transfer in Aqueous Nafion Proton-Exchange- Membrane Nanochannels. *Phys. Rev. Lett.* **2014**, *112*, 1−5.
(63) Liu, L.; Bakker, H. J. Vibrational Excitation Induced Proton Transfer in Hydrated Nafion Membranes. *J. Phys. Chem. B* **2015**, *119*, 2628−2637.
(64) Liu, L.; Lotze, S.; Bakker, H. J. Vibrational and Structural Relaxation of Hydrated Protons in Nafion Membranes. *Chem. Phys. Lett.* **2017**, *670*, 102−108.
(65) Cao, Z.; Peng, Y.; Yan, T.; Li, S.; Li, A.; Voth, G. A. Mechanism of Fast Proton Transport along One-Dimensional Water Chains Confined in Carbon Nanotubes. *J. Am. Chem. Soc.* **2010**, *132*, 11395−11397.
(66) Dellago, C.; Naor, M. M.; Hummer, G. Proton Transport through Water-Filled Carbon Nanotubes. *Phys. Rev. Lett.* **2003**, *90*, 105902.
(67) Galama, A. H.; Vermaas, D. A.; Veerman, J.; Saakes, M.; Rijnaarts, H. H. M.; Post, J. W.; Nijmeijer, K. Membrane Resistance: The Effect of Salinity Gradients over a Cation Exchange Membrane. *J. Membr. Sci.* **2014**, *467*, 279−291.
(68) Volodina, E.; Pismenskaya, N.; Nikonenko, V.; Larchet, C.; Pourcelly, G. Ion Transfer across Ion-Exchange Membranes with Homogeneous and Heterogeneous Surfaces. *J. Colloid Interface Sci.* **2005**, *285*, 247−258.
(69) Kreuer, K. D. *J. Membr. Sci.* **2001**, *185*, 29−39.
(70) Rollet, A.-L.; Diat, O.; Gebel, G. A New Insight into Nafion Structure. *J. Phys. Chem. B* **2002**, *106*, 3033−3036.
(71) Markovic, N. M. Electrocatalysis: Interfacing Electrochemistry. *Nat. Mater.* **2013**, *12*, 101−102.
(72) Spurgeon, J. M.; Lewis, N. S. Proton Exchange Membrane Electrolysis Sustained by Water Vapor. *Energy Environ. Sci.* **2011**, *4*, 2993.
(73) Spurgeon, J. M.; Walter, M. G.; Zhou, J.; Kohl, P. A.; Lewis, N. S. Electrical Conductivity, Ionic Conductivity, Optical Absorption, and Gas Separation Properties of Ionically Conductive Polymer Membranes Embedded with Si Microwire Arrays. *Energy Environ. Sci.* **2011**, *4*, 1772.
(74) Xiang, C.; Chen, Y.; Lewis, N. S. Modeling an Integrated Photoelectrolysis System Sustained by Water Vapor. *Energy Environ. Sci.* **2013**, *6*, 3713.
(75) Gasteiger, H. A.; Panels, J. E.; Yan, S. G. Dependence of PEM Fuel Cell Performance on Catalyst Loading. *J. Power Sources* **2004**, *127*, 162−171.
(76) Daimler. *Under the microscope: Mercedes-Benz GLC F-CELL*. http://media.daimler.com/marsMediaSite/en/instance/ko.xhtml?oid=11111320. (accessed Oct 9, 2017).
(77) Keeley, G. P.; Cherevko, S.; Mayrhofer, K. J. J. The Stability Challenge on the Pathway to Low and Ultra-Low Platinum Loading for Oxygen Reduction in Fuel Cells. *ChemElectroChem* **2016**, *3*, 51−54.
(78) Cherevko, S.; Geiger, S.; Kasian, O.; Kulyk, N.; Grote, J. P.; Savan, A.; Shrestha, B. R.; Merzlikin, S.; Breitbach, B.; Ludwig, A.; et al. Oxygen and Hydrogen Evolution Reactions on Ru, RuO_2, Ir, and IrO_2 Thin Film Electrodes in Acidic and Alkaline Electrolytes: A Comparative Study on Activity and Stability. *Catal. Today* **2016**, *262*, 170−180.

DOI: 10.1021/acsenergylett.7b00764
ACS Energy Lett. 2017, 2, 2625−2634

(79) Cherevko, S.; Geiger, S.; Kasian, O.; Mingers, A.; Mayrhofer, K. J. J. Oxygen Evolution Activity and Stability of Iridium in Acidic Media. Part 1. - Metallic Iridium. *J. Electroanal. Chem.* **2016**, *773*, 69−78.
(80) Cherevko, S.; Geiger, S.; Kasian, O.; Mingers, A.; Mayrhofer, K. J. J. Oxygen Evolution Activity and Stability of Iridium in Acidic Media. Part 2. - Electrochemically Grown Hydrous Iridium Oxide. *J. Electroanal. Chem.* **2016**, *774*, 102−110.
(81) Cherevko, S.; Kulyk, N.; Mayrhofer, K. J. J. Durability of Platinum-Based Fuel Cell Electrocatalysts: Dissolution of Bulk and Nanoscale Platinum. *Nano Energy* **2016**, *29*, 275−298.
(82) Cherevko, S.; Keeley, G. P.; Kulyk, N.; Mayrhofer, K. J. J. Pt Sub-Monolayer on Au: System Stability and Insights into Platinum Electrochemical Dissolution. *J. Electrochem. Soc.* **2016**, *163*, H228−H233.
(83) Varcoe, J. R.; Atanassov, P.; Dekel, D. R.; Herring, A. M.; Hickner, M. A.; Kohl, P. A.; Kucernak, A. R.; Mustain, W. E.; Nijmeijer, K.; Scott, K.; et al. Anion-Exchange Membranes in Electrochemical Energy Systems. *Energy Environ. Sci.* **2014**, *7*, 3135−3191.
(84) Merle, G.; Wessling, M.; Nijmeijer, K. Anion Exchange Membranes for Alkaline Fuel Cells: A Review. *J. Membr. Sci.* **2011**, *377*, 1−35.
(85) Arges, C. G.; Ramani, V.; Pintauro, P. N. Anion Exchange Membrane Fuel Cells. *Electrochem. Soc. Interface* **2010**, *31*, 31−35.
(86) Chinen, H.; Mawatari, K.; Pihosh, Y.; Morikawa, K.; Kazoe, Y.; Tsukahara, T.; Kitamori, T. Enhancement of Proton Mobility in Extended-Nanospace Channels. *Angew. Chem., Int. Ed.* **2012**, *51*, 3573−3577.
(87) Pihosh, Y.; Uemura, J.; Turkevych, I.; Mawatari, K.; Kazoe, Y.; Smirnova, A.; Kitamori, T. From Extended Nanofluidics to an Autonomous Solar-Light-Driven Micro Fuel-Cell Device. *Angew. Chem., Int. Ed.* **2017**, *56*, 8130−8133.
(88) McDonald, M. B.; Ardo, S.; Lewis, N. S.; Freund, M. S. Use of Bipolar Membranes for Maintaining Steady-State pH Gradients in Membrane-Supported, Solar-Driven Water Splitting. *ChemSusChem* **2014**, *7*, 3021−3027.
(89) Vermaas, D. A.; Smith, W. A. Synergistic Electrochemical CO_2 Reduction and Water Oxidation with a Bipolar Membrane. *ACS Energy Lett.* **2016**, *1*, 1143−1148.
(90) Vargas-Barbosa, N. M.; Geise, G. M.; Hickner, M. A.; Mallouk, T. E. Assessing the Utility of Bipolar Membranes for Use in Photoelectrochemical Water-Splitting Cells. *ChemSusChem* **2014**, *7*, 3017−3020.
(91) Winger, A. G.; Bodamer, G. W.; Kunin, R. Some Electrochemical Properties of New Synthetic Ion Exchange Membranes. *J. Electrochem. Soc.* **1953**, *100*, 178−184.
(92) Peng, S.; Lu, S.; Zhang, J.; Sui, P.-C.; Xiang, Y. Evaluating the Interfacial Reaction Kinetics of the Bipolar Membrane Interface in the Bipolar Membrane Fuel Cell. *Phys. Chem. Chem. Phys.* **2013**, *15*, 11217.
(93) Peng, S.; Xu, X.; Lu, S.; Sui, P. C.; Djilali, N.; Xiang, Y. A Self-Humidifying Acidic-Alkaline Bipolar Membrane Fuel Cell. *J. Power Sources* **2015**, *299*, 273−279.
(94) Emrén, A. T.; Holmström, V. J. M. Energy Storage in a Fuel Cell with Bipolar Membranes Burning Acid and Hydroxide. *Energy* **1983**, *8*, 277−282.
(95) O'Hayre, R.; Barnett, D. M.; Prinz, F. B. The Triple Phase Boundary. *J. Electrochem. Soc.* **2005**, *152*, A439.
(96) Schoemaker, M.; Misz, U.; Beckhaus, P.; Heinzel, A. Evaluation of Hydrogen Crossover through Fuel Cell Membranes. *Fuel Cells* **2014**, *14*, 412−415.
(97) Inaba, M.; Kinumoto, T.; Kiriake, M.; Umebayashi, R.; Tasaka, A.; Ogumi, Z. Gas Crossover and Membrane Degradation in Polymer Electrolyte Fuel Cells. *Electrochim. Acta* **2006**, *51*, 5746−5753.
(98) Feldmann, F.; Simon, M.; Bivour, M.; Reichel, C.; Hermle, M.; Glunz, S. W. Carrier-Selective Contacts for Si Solar Cells. *Appl. Phys. Lett.* **2014**, *104*, 181105.
(99) Koswatta, P.; Boccard, M.; Holman, Z. Carrier-Selective Contacts in Silicon Solar Cells. *Photovolt. Spec. Conf. (PVSC)*, 2015 IEEE 42nd; 2015; pp 1−4.
(100) Bassignana, I. C.; Reiss, H. Ion Transport and Water Dissociation in Bipolar Ion Exchange Membranes. *J. Membr. Sci.* **1983**, *15*, 27−41.
(101) Mafé, S.; Manzanares, J. A.; Ramrez, P. Model for Ion Transport in Bipolar Membranes. *Phys. Rev. A: At., Mol., Opt. Phys.* **1990**, *42*, 6245−6248.
(102) Conroy, D. T.; Craster, R. V.; Matar, O. K.; Cheng, L. J.; Chang, H. C. Nonequilibrium Hysteresis and Wien Effect Water Dissociation at a Bipolar Membrane. *Phys. Rev. E - Stat. Nonlinear, Soft Matter Phys.* **2012**, *86*, 1−10.
(103) Kaiser, V.; Bramwell, S. T.; Holdsworth, P. C. W.; Moessner, R. Onsager's Wien Effect on a Lattice. *Nat. Mater.* **2013**, *12*, 1033−1037.
(104) Gabbasa, M.; Sopian, K.; Fudholi, A.; Asim, N. A Review of Unitized Regenerative Fuel Cell Stack: Material, Design and Research Achievements. *Int. J. Hydrogen Energy* **2014**, *39*, 17765−17778.
(105) Soloveichik, G. L. Regenerative Fuel Cells for Energy Storage. *Proc. IEEE* **2014**, *102*, 964−975.
(106) Hewa Dewage, H.; Wu, B.; Tsoi, A.; Yufit, V.; Offer, G.; Brandon, N. A Novel Regenerative Hydrogen Cerium Fuel Cell for Energy Storage Applications. *J. Mater. Chem. A* **2015**, *3*, 9446−9450.
(107) Dewage, H. H.; Yufit, V.; Brandon, N. P. Study of Loss Mechanisms Using Half-Cell Measurements in a Regenerative Hydrogen Vanadium Fuel Cell. *J. Electrochem. Soc.* **2016**, *163*, A5236−A5243.
(108) Lucas, J.; Bockstahler, K.; Funke, H.; Jehle, W.; Markgraf, S.; Henn, N.; Schautz, M. Regenerative Fuel Cell System As Alternative Energy Storage for Space. In *Proc. "9th European Space Power Conference"*, Saint Raphaël, France; 2011; Vol. 2011; pp 6−10.
(109) Bolwin, K. Application of Regenerative Fuel Cells for Space Energy Storage: A Comparison to Battery Systems. *J. Power Sources* **1992**, *40*, 307−321.

DOI: 10.1021/acsenergylett.7b00764
ACS Energy Lett. 2017, 2, 2625−2634